Published in final edited form as:
Biomaterials. 2009 March ; 30(7): 1299–1308. doi:10.1016/j.biomaterials.2008.11.018.

Silk film biomaterials for cornea tissue engineering

Brian D. Lawrence[1], **Jeffrey K. Marchant**[2], **Mariya Pindrus**[1], **Fiorenzo Omenetto**[1,3], and **David L. Kaplan**[1]

1 *Department of Biomedical Engineering, Tufts University, 4 Colby St., Medford, MA, 02155, USA*

2 *Department of Molecular, Cell, and Developmental Biology, Tufts University, 136 Harrison Ave., Boston, MA, 02111, USA*

3 *Department of Physics and Astronomy, Tufts University, 4 Colby St., Medford, MA 02155, USA*

Abstract

Biomaterials for corneal tissue engineering must demonstrate several critical features for potential utility *in vivo*, including transparency, mechanical integrity, biocompatibility and slow biodegradation. Silk film biomaterials were designed and characterized to meet these functional requirements. Silk protein films were used in a biomimetic approach to replicate corneal stromal tissue architecture. The films were 2 μm thick to emulate corneal collagen lamellae dimensions, and were surface patterned to guide cell alignment. To enhance trans-lamellar diffusion of nutrients and to promote cell-cell interaction, pores with 0.5 to 5.0 μm diameters were introduced into the silk films. Human and rabbit corneal fibroblast proliferation, alignment and corneal extracellular matrix expression on these films in both 2D and 3D cultures was demonstrated. The mechanical properties, optical clarity and surface patterned features of these films, combined with their ability to support corneal cell functions suggest this new biomaterial system offers important potential benefits for corneal tissue regeneration.

Keywords

Biomimetic material; Cornea; Fibroblast; Porosity; Scaffold; Silk; Surface topography

1. Introduction

Corneal blindness accounts for nearly 10 million cases of vision loss worldwide [1]. Corneal grafts are the most commonly performed tissue transplant in the US, with 30,000 to 40,000 performed annually [1]. Corneal graft rejection rate is below 10%, however by 4–5 years post implantation the immunological rejection rate increases to 25% and continues to increase over the life of the patient [2,3]. Currently the only alternative to allograft tissue replacements are synthetic keratoprosthesis, however, these also exhibit a relatively high host rejection rate [4, 5]. Therefore, new biomaterial options are needed for the development of clinical devices for corneal replacements. Current research efforts have focused on employing hydrogel materials to mimic the corneal architecture, in which cross-linked collagen gels have shown some success in animal models [6–10]. Further work has been undertaken to produce cell sheets of cornea tissue, which have been utilized for corneal epithelial repairs [9,11]. More recent efforts have

been underway to construct magnetically aligned collagen fibrils to produce an analog to the corneal stroma matrix [12]. Initial studies have shown the successful culturing of 3D scaffolds that promote cell alignment along the orthogonally stacked fibril layers. However, the production of a fully functional corneal construct has not been demonstrated to date, and new approaches should continue to be developed to increase the biomaterial options available for corneal tissue repair.

Silk fibroin is the structural protein obtained from the cocoon of the silk worm *Bombyx mori*. Silk proteins represent a unique choice in biomaterial selection for tissue engineering and regenerative medicine applications due to fibroin's non-immunogenic response upon *in vivo* implantation, controllable material degradation rates, tunable and robust mechanical properties, and ambient aqueous processing [13–19]. Silk fibroin cast into film form can be embedded with labile cell-signaling molecules to generate biologically functional matrices [20–23]. In addition, silk film surfaces can be patterned using soft lithographic techniques to produce high resolution surface features [20,24,25]. Topographic patterning has been found to play a role in epithelial and fibroblast alignment, adhesion, mobility, and proliferation [26–31]. In addition, silk substrates have been shown to support human limbal epitheial stem cell attachment and proliferation on a comparable scale to tissue culture plastic [32]. However, further work is needed to characterize both corneal fibroblast and endothelium growth upon these substrates. Furthermore, patterned silk biomaterials combined with their inherent optical clarity [16,32] provide a new approach to generate useful surfaces for directing cellular function and matrix deposition, while matching mechanical and optical functional needs for corneal tissue engineering. Such material properties are especially relevant for corneal fibroblast growth, which produce aligned collagen lamellae that are combined together to create a robust and transparent tissue architecture [33–35]. Patterned silk films may be used to provide contact guidance to produce aligned cellular matrices, while also providing a robust and transparent scaffold structure to support native tissue regeneration.

In the present study, optically transparent surface patterned thin silk films were prepared and studied to determine their suitability for rabbit and human corneal fibroblast culture. A rabbit cornea cell line expressing the green fluorescent protein (GFP-rCF) was generated to assess cell morphology and alignment on the silk surfaces. Subsequently, a human corneal fibroblast (hCF) cell line [6] was seeded on film surfaces, followed by film stacking, to generate biomimetic 3D lamellar corneal tissue constructs.

2. Materials and Methods

2.1. Preparation of silk solution

As described previously [36], *Bombyx mori* silk cocoons (Institute of Sericulture, Tsukuba, Japan) were cut into fourths and then boiled for 45 minutes in 0.02M Na_2CO_3 (Sigma-Aldrich) to extract the glue-like sericin proteins from the structural fibroin proteins. The fibroin extract was then rinsed three times in Milli-Q water, dissolved in 9.3M LiBr solution at room-temperature, and set covered within a 60°C oven for 4 hours. The solution was then dialyzed (MWCO 3500) in water for 48hrs. The dialyzed silk solution was then centrifuged at 13,000 g, and the supernatant was collected and stored at 4°C. The final concentration of aqueous silk solution was 8 wt/vol.%, as determined by gravimetric analysis.

2.2. Preparation of polydimethylsiloxane (PDMS) substrates

Flat and patterned PDMS (GE Plastics) substrates of 0.5–1.0 mm thickness were prepared by casting on flat optical mirror and 600 lines/mm diffraction grating (Edmund Optics, Inc.) surfaces respectively. PDMS rounds were punched with 14 mm diameters. The PDMS substrates were placed cast side up, and prepared for silk casting by a 70% ethanol wash with

three DI water washes. PDMS surfaces were used for multiple silk film castings using an additional 9.3M LiBr soaking washing step with subsequent ethanol and DI water rinsing.

2.3. Preparation of silk films

100 uL of 8% silk solution was cast upon both flat and grooved PDMS substrates 14 mm in diameter to give a 40 μm film thickness. The films were then covered with a venting lid, and allowed to dry overnight. In addition, silk solution was cast upon polycarbonate diffractive optical patterns (Tessera, Inc., San Jose, CA) to create circular geometries upon the silk films surface. Once dried, water-annealing processing was performed by placing the silk films within a water-filled desiccator, a 24 mm Hg vacuum was pulled, and then the films were left within the water vapor environment for a five hour period. The silk films were immersed in water baths and removed from their PDMS substrates. Films were then placed into 12-well plates, and laid flat against the well bottoms. The wells were then filled with 70% EtOH to disinfect the films for cell culture. Each film was then washed three times in ultrapure dH_2O. The wells were then filled with 1 mL of media in preparation for cell seeding.

2.4. Preparation of porous silk films

A mixture of 1% silk fibroin and 0.05% polyethylene oxide (PEO, MW_v=900,000; Sigma-Aldrich) solutions was prepared to induce pore formation within the silk film matrix. 100 μL of solution was cast on flat PDMS substrates as described above to produce 2 μm film thicknesses. Post-casting, silk films were water-annealed and then placed into a water bath for 24 hours to leach out the PEO phase. The films were transferred into 12-well plates and sterilized using 70% EtOH. Three film samples were sputter coated with gold for SEM imaging.

2.5. Generation of green fluorescent protein (GFP) expressing rCFs

Primary stromal keratocytes were isolated from excised rabbit corneas (Pel-Freeze, Rogers, AR) as previously described in accordance with ethical regulations [37] and cultured in rabbit fibroblast media (rFB) consisting of Dulbecco's modified Eagle's medium (DMEM), 10% fetal bovine serum (FBS), 1% penicillin-streptomycin-fungizone (PSF), and maintained at 5% CO_2. A GFP-expressing line of rCFs (GFP-rCFs) was generated using a previously described lentivirus system [38]. rCFs were transduced at multiplicity of infection (MOI) 10–50, with five milliliters of virus-containing supernatant (100,000 virus particles/mL) added to $5x10^5$ rCFs. An additional 5mL of rFB media was added in the flask along with protamine sulfate (6 mg/mL) to enhance the infection. The cells were incubated for 3 h with the lentivirus, and then washed twice with PBS before adding rFB media. The efficiency of GFP transduction was evaluated through fluorescence microscopy and fluorescence-activated cell sorting (FACS) analysis (BD, Franklin Lakes, NJ). Stable GFP-rCFs were determined by the presence of fluorescence in the cells over multiple cell passages. For seeding, GFP-rCFs were grown to confluence, detached from their substrates using 0.25% Trypsin (Gibco), and then replated at passage 7 (P7) onto silk films and tissue-culture plastic (TCP) at a density of 5,000 cells/cm^2. GFP-rCFs were then monitored using fluorescent microscopy over a two week culture period. Fluorescent excitation wavelengths were at 488 nm with collected emission wavelengths of 500–560 nm.

2.6. Transfected human cell culture and film seeding

P7 immortalized human corneal keratocytes (hCF) were kindly provided by May Griffith (University of Ottawa Eye Institute). Human cell lines were isolated from donor corneas, and immortalized by infection with an amphotropic recombinant retrovirus containing HPV16 genes E6 and E7 and with mammalian expression vectors containing genes encoding SV40 large T antigen, pSV3neo, and adenovirus E1A 12S as described previously [6]. Cultures were grown to confluence using human fibroblast media (hFB) consisting of DMEM, 10% FBS, 1%

interferon-transferrin-selenium (ITS), and 1% PSF (Gibco), and used for experimentation at P9. The cultures were detached from their substrates using 0.25% Trypsin (Gibco), and then replated on silk films and TCP at a density of 5,000 cells/cm^2.

2.7. DNA content assay

DNA content was assessed using the Pico Green assay (Invitrogen, Inc.). Samples were incubated in 1 mL of 0.1% Triton-X 100 in 1xTE buffer for 48 hours. The sample supernatant was spun down by centrifugation for 5 minutes. After centrifugation a 25 μL aliquot of supernatant was taken from each sample and placed into 96-well plate with wells containing 75 μL of 1xTE buffer. A standard curve was generated using lambda phage DNA in 0, 2.5, 5, 10, and 25-ug/mL concentrations. One hundred μL of a 1:200 dilution of Quant-iT PicoGreen (Invitrogen, Inc.) reagent was added to each well and read using a fluorimeter with an excitation wavelength of 480 nm and an emission wavelength of 520 nm. ANOVA and post hoc Student t-tests were performed to compare the mean DNA content values between substrate groups and between time points (n=6). Statistical significance was demonstrated for $p<0.05$.

2.8. Immunohistological staining

After two weeks in culture sample media was removed and cultures were washed two times with PBS. The samples were then fixed for ten minutes at room temperature using 4% paraformaldehyde solution. The 4% paraformaldehyde was removed with 3 subsequent PBS washings. Actin filaments were stained using Texas Red-X phalloidan stain (Molecular Probes, Inc.), and was diluted using 10 μL of methanolic stock reagent and 400 μL of PBS for each sample. After diluting, 410 μL was placed onto each sample for 30 minutes with two subsequent PBS rinses. Primary antibodies for collagen V, vimentin, and keratin (Chemicon, Inc.) were diluted from their respective stock solutions to 5–10 μg/mL concentrations in PBS. 400 μL of antibody solution was placed onto each sample and left to sit at room temperature for two hours. The samples were then washed two times with PBS. Alexafluor 488 (human) or 546 (rabbit) (Invitrogen, Inc.) was used for secondary antibody staining, in which a 10 μg/mL dilution was prepared. 400 μL of secondary antibody solution was added to each sample for 30 minutes with 2 subsequent PBS rinses. All samples were mounted onto glass slides using Prolong anti-fading mounting media with 4',6-diamidino-2-phenylindole (DAPI) (Invitrogen, Inc.).

2.9. Fluorescent imaging of cell seeded silk films and cell alignment analysis

Fluorescent microscopy was performed for 2D cultures. Silk substrate excitation was at 400 nm and collected emission between 420–520 nm; phalloidan staining excitation was at 595 nm and collected emission between 605–650 nm; and Alexafluor secondary antibody excitation was at 488 nm or 546 nm and collected emission between 500–560 or 565–585 nm, respectively. A 488/543 dichroic was used for phalloidan and Alexafluor. Actin filament and collagen alignment was assessed using MATLAB to assess feature orientation using the power spectral density (PSD) of each image [39,40]. Post hoc statistical analysis was carried out using Student t-tests ($p<0.05$; n=3). Fluorescent confocal microscopy was used for 3D construct imaging, and z-stack images were generated using Leica imaging software (Leica, Inc.).

2.10. SEM preparation and imaging

Sample media was removed from each culture well with 2 subsequent PBS rinses. Samples were fixed using 2.5% glutaraldehyde in 0.1M Cacodylate buffer with 0.1M sucrose and 4 mM $CaCl_2$, pH 7.4 (Electron Microscopy Sciences), and let to sit overnight at 4° Celsius. The next day, fixative was removed with 3 subsequent 0.1M Sodium Cacodylate buffer with 0.1M sucrose and 4mM $CaCl_2$ (Electron Microscopy Sciences) rinses. Samples were dehydrated using 50, 70, 85, 95 and 100% ethanol serial dilution steps. Samples were dried overnight in

ambient conditions. The following day, samples were washed twice with hexamethyldisilazane (HMDS) solvent (Electron Microscopy Sciences) and placed within a desiccator. Samples were sputter coated with a 40 nm layer of gold and imaged using a JEOL JSM 840-A SEM.

2.11. Stacked porous silk film stacking cell seeding procedure

Prepared porous silk films were presoaked with hCF media for 30 minutes. Confluent cell cultures were detached from their TCP substrates using 0.25% trypsin (Gibco, Inc.). Cells were then seeded upon the porous silk films at 100,000 cells/cm^2 seeding density and left to incubate for 24 hours to allow for cell attachment. Seeded porous films were then carefully stacked into 12-well plates. A total of 7 films were stacked per construct in each well, and then the stacks were sealed together using applied pressure from a 12 mm biopsy punch. The applied pressure was used to seal the stacked film construct together near the film edges, but did not pierce through the silk film substrate. Phase contrast images of the films were taken every 2 days, and confocal imaging of fixed and stained constructs was performed at day 7 as described above.

3. Results

3.1. Cell alignment, morphology, and proliferation upon silk film substrates

Circle patterned silk film surfaces (Fig. 1a,b) were cast from patterned polycarbonate molds, seeded with GFP-rCFs, and cultured *in vitro* for 1 week. GFP-rCFs aligned with the concentric circular patterned silk surfaces on both 700 μm and 1 cm diameter lens scales (Fig. 1c,d). A variety of cell morphologies were observed on the larger 1 cm concentric circular pattern (Fig. 1c) that corresponded to different regions of the patterned silk film surface. GFP-rCFs located in the center region exhibited spread morphologies while GFP-rCFs located on the outer circular edges were more elongated and well aligned to the patterned radial arc. Although circular cell geometries are not found in the cornea tissue architecture, the cell circle patterns provide a striking visual demonstration of how cell alignment is greatly influenced by the presented pattern of the silk film substrate.

To provide a more relevant cell guiding substrate for corneal tissue engineering, linear groove patterns (Fig. 2a) and flat (Fig. 2c) silk film surfaces were generated to better assess directed corneal fibroblast cell alignment. Previous studies have demonstrated that grooved surface patterning promotes cell alignment on tissue culture plastic, surface treated PDMS, titanium, and silicon [25,30,31]. Silk film surfaces with patterned features of 6.6 μm groove widths guided primary fibroblast alignment [25].

The linear groove patterns (Fig. 2b) were generated using a soft lithography approach [41], and measured 1.67 μm peak to peak with an 8° angled 200 nm pitch. These dimensions correlate with previous studies using similar patterned surfaces to promote corneal fibroblast alignment [11,28,42]. Flat silk film surfaces (Fig. 2d) were generated by casting silk solution onto flat PDMS surfaces generated from optical glass mirrors.

Porous silk films were generated by casting a mixture of silk and PEO solution onto both patterned and flat PDMS substrates. The silk and PEO phase separate to produce PEO aggregates within the bulk aqueous silk phase [36,43]. PEO aggregation within macromolecule solutions has been previously described [44]. The silk films were then dried and water-annealed by incubation within a water saturated vacuum environment to induce increased β-sheet formation that produces water insoluble films [16,20]. After water-annealing, the films were then placed within a water bath for 24 hours to leach out the PEO aggregate phase. This is accomplished due to the silk phase becoming water insoluble post water-annealing, while the PEO phase remaining water soluble. Upon dissolution of the PEO aggregates within the water bath, porous voids are left behind within the bulk silk matrix with pore size ranging between

500 nm – 5 μm in diameter (Fig. 2ef). By producing thin silk films 2 μm in thickness porous structures could be produced that extend through the film bulk. The combination of porous and thin silk films allows for the construction of lamellae-like tissue scaffolds that can be assembled together to produce a three-dimensional tissue construct.

GFP-rCFs were cultured on both the linear groove patterned and flat silk film surfaces for two weeks. Fluorescent imaging of the GFP expressing fibroblasts demonstrated that cell alignment was evident two days post-seeding (Fig. 3a), in contrast to the random growth on the unpatterned films (Fig. 3d). At day 10 in culture the patterned silk surfaces exhibited aligned confluent cell coverage (Fig. 3b), while the unpatterned surfaces demonstrated confluent random growth (Fig. 3e). SEM imaging revealed elongated spindle-like GFP-rCF morphology aligning along the groove axis of the patterned surfaces (Fig. 3c), while in contrast the unpatterned films solicited spread cellular morphologies (Fig. 3f). In addition, the GFP-rCFs appeared aggregated and mounded on the flat silk film surfaces while the patterned surface cultures exhibit reduced cell density and more evenly spaced cellular bodies. Strong cell attachment to the silk film surface seemed apparent on both surfaces (Fig. 3cf). Defined focal adhesion points were present on the patterned silk surfaces and appeared to apply a tensional force upon the aligned cell bodies (Fig. 3c). This was opposed to the spreading of GFP-rCFs on the flat silk surfaces which appeared to apply less tensional forces when compared to patterned surfaces (Fig. 3f).

DNA content was measured in GFP-rCF grown on both flat and patterned silk surfaces as well as on tissue culture plastic (TCP) over a six day period (Fig. 3g). DNA content increased with time for all substrate conditions. GFP-rCF DNA content was significantly lower on day 6 for the patterned silk substrates when compared to TCP. The patterned silk surfaces also exhibited a decreasing trend in average DNA content when compared to flat silk surfaces. In addition, the patterned silk surfaces exhibited a trend of possessing the lowest DNA content throughout the culture period. These results suggest that GFP-rCF DNA content is altered by the patterned surface. The influence of patterned surfaces on corneal fibroblast DNA content *in vitro* has been previously shown for grooved geometries on various silicone substrates [28,29]. This decrease in DNA content may be related to the adhesion strength of the …..

3.2. Cytoskeletal organization and extracellular matrix (ECM) expression upon silk film substrates

GFP-rCF cellular processes aligned along the direction of the silk film patterned groove axis and were up to 2.5 times the cell body length (Fig. 4a). Fluorescent imaging confirmed that these processes were cellular based from the presence of GFP signal (Fig. 4b). GFP-rCF actin was stained with phalloidan to show that actin filaments were aligned along the patterned groove axis (Fig. 4g), in contrast to actin formation on the flat silk film surfaces (Fig. 4h). Additionally, actin filaments were highly aligned with the cell processes. Cultures growing on the flat silk film surfaces exhibited a less organized growth pattern, based on the random alignment of both actin filaments and cell bodies. These results agree with previous findings that directional actin filament organization due to contact guidance corresponds to increased cellular alignment along the pattern axis [28,29,39].

To quantify the level of cytoskeletal alignment on the patterned and flat silk film surfaces, orientation was calculated based on the power spectral density (PSD) of the images[39,40]. Statistical analysis showed that actin filaments showed significantly more alignment on patterned silk film surfaces (Fig. 4i). These results indicate that the silk film patterned structures significantly impacted cytoskeletal alignment. Fluorescent imaging of the actin filaments showed changes in cell morphology and alignment based on cell density over time on the different silk film surfaces (Fig. 4bc). GFP-rCFs exhibited greater spreading and decreased actin filament alignment on the patterned film surfaces at lower cell densities. As cell density

increased, cellular morphology became more compact and the actin filaments became highly oriented in the groove direction. A statistically significant increase in alignment was found at higher cell densities for the patterned silk films (Fig. 4i). On the flat silk film surfaces cell morphology was more spread at lower cell density (Fig. 4ef) and overall alignment did not change at different cell densities (Fig. 4i). These results indicate that patterned silk film surfaces have a greater impact on directing actin alignment during culture development over time.

Collagen type V is expressed at high levels in the cornea [45]. We observed collagen type V expression by the GFP-rCF on the silk substrates (Fig. 5ae). High collagen type V expression is characteristic of the corneal fibroblast phenotype and aids in regulating collagen fibril diameter [46]. Collagen type V was expressed on both patterned and unpatterned silk film surfaces. These results indicate that the seeded corneal fibroblasts retained their differentiated phenotype while cultured on the silk films. In addition, cells bodies are seen to align upon the patterned silk film surfaces (Fig. 5a) when compared to flat silk surfaces (Fig. 5e). In a wound healing response, corneal fibroblasts differentiate into a myofibroblast phenotype that do not highly express collagen type V [47]. Therefore, expression of collagen type V is an indicator of native ECM formation vs. scar formation on the silk substrates. Vimentin was also expressed as a positive control on both silk substrates (Fig. 5bf), while no keratin (epithelium marker) (Fig. 5cg) or non-specific secondary antibody binding to silk was observed (Fig. 5dh). These results indicate that collagen type V production is retained upon both patterned and flat silk film surfaces, thus indicating the retention of the corneal fibroblast phenotype.

3.3. Three-dimensional silk film tissue construct

To assess the use of silk films for use as three dimensional constructs an immortalized hCF cell line was used. This cell line was chosen over the GFP-rCF primary cells because they have been shown to be successfully cultured in 3D scaffolds, and have been engineered to possess a distinct spread and flattened keratocytes morphology when cultured *in vitro* within non-confluent cultures [6]. Therefore, the presence of spread cell morphology was used as a visual marker for the retainment of cell phenotype in culture as this has been previously described in the literature [6]. Collagen V expression was not used with this cell line due to technical difficulties with potential staining of the assembled silk film construct , therefore visual spreading was a consistent marker between both 2D and 3D platforms.

Cell attachment to the silk films was initially tested on 2D silk film surfaces by seeding hCFs onto films fabricated as described above. hCF were cultured on both patterned and unpatterned silk film substrates and assessed by phase contrast imaging (Fig. 6a–d). Cell attachment and some alignment of the cell body along the groove axis on the patterned silk films were apparent by day 3 inculture (Fig. 6a). However, the cell alignment was not as distinct for hCFs when compared with the GFP-rCF cultures. Confluent cultures showed some alignment with the patterned groove axis near cell confluency at day 7 (Fig. 6b), however the alignment was not as apparent when compared with GFP-rCF cultures. Similar cell adhesion and increased random cell growth was seen for flat silk surfaces at day 3 (Fig. 6c), however sections of aligned cell growth were apparent in areas of confluent cultures (Fig. 6d). The decrease in cell alignment along the groove axis was somewhat anticipated, as this cell line was designed to maintain a spread morphology *in vitro* as opposed to elongated morphologies exhibited by primary corneal fibroblasts like the GFP-rCFs *in vitro* [6].

The DNA content of hCFs cultured upon both silk film surfaces and TCP was observed to increase on all substrates over one week (Fig. 6e). Both patterned and non-patterned silk film surfaces supported similar increases in DNA content on day 3, while TCP cultures exhibited a statistically significant increase at day 3. On day 5 all three culture substrates were statistically different and by day 7 TCP cell growth reached a plateau corresponding with confluency. Both silk film surfaces maintained increases in DNA content between days 5 and 7, and the flat silk

surfaces exhibited a trend of increased DNA content when compared to the patterned silk substrates. The patterned silk surface cultures exhibited a trend for exhibiting the lowest DNA content for all substrates, which correlates with the previous GFP-rCF results.

Silk films were then assembled to construct a three-dimensional lamellar scaffold to mimic the stromal layer of the cornea. The films were 2 μm in thickness and contained pores ranging from 500 nm to 5 μm in diameter as described above (Fig 2e–g). Pores were introduced to aid in nutrient diffusion and cell-cell contact through the stacked construct. hCFs were seeded on the silk films prior to stacking and incubated for 24 hours to allow for initial cell adhesion (Fig. 7b). Subsequently, seven cell seeded silk films were assembled to produce the lamellar construct. The silk films were stacked upon one another, and then their lamellae edges were sealed together using applied pressure from a 12 mm biopsy bunch through hydrostatic bonding (Fig. 7a) as we have described previously [24]. The stacked films were incubated for 1 week and then fixed for immunostaining and imaging by confocal microscopy for actin (Fig. 7ef) and collagen type I (Fig. 6g). The samples were then prepared for SEM to image morphological features of the stacked construct (Fig. 7cd).

Observed fluorescent actin staining throughout the stacked silk film construct indicated that the cells were viable and organized throughout the entire structure (Fig. 7e). hCFs interacted with multiple silk film surfaces (Fig. 7f) and maintained a spread phenotype similar to that of *in situ* corneal keratocytes [48]. It has been previously shown that primary human corneal fibroblasts in collagen gel matrices exhibit this same spread morphology [48]. Cell spreading has been attributed to the interaction of both the apical and basal cellular surfaces with the surrounding matrix, thus a similar cellular interaction may be taking place within the assembled silk layers. However, cell alignment was not readily apparent by 1 week in culture and may be due to the inherent ability of the hCF spreading. Collagen type I antibody staining demonstrated that collagen matrix was present throughout the construct (Fig. 7g). These results demonstrate that 2 μm thin porous silk films may be constructed to form a three-dimensional scaffold to support both corneal cell viability and corneal tissue matrix production.

SEM imaging of cross-sections showed morphological features of the assembled silk film corneal tissue construct (Fig. 7cd). The assembled structures showed adequate spacing between the film layers to allow for cell growth and tissue development. Regions of the silk film surface appeared to be covered by cells and native ECM (Fig. 7c). Higher magnification demonstrated cells interacting with multiple silk film surfaces and the pores (Fig. 7d). These images indicate that the assembled construct maintains cell viability and structural integrity after seven days in culture.

4. Discussion

Optically transparent self-standing thin silk film biomaterials were formed and utilized to culture both rCF and hCF cells. Both cell types showed increased proliferation over time on both flat and patterned silk film surfaces, with differences in cellular morphologies between the two types of surfaces. Actin filament organization was also influenced by the presence of the surface patterning. These results indicate that patterned silk film surfaces may be designed to direct cell responses. Surface patterning has been shown to impact corneal cell function [28,42,49]. The results in the present work demonstrated that patterned silk films provided a suitable environment to control cell alignment and promote native ECM synthesis, The use of surface patterning may be teamed with coupling of bioactive molecules to the silk surface to further control material-cell interactions, thus offering a highly tailored biomaterials approach to implantable medical devices [16,19,36,50]. The combination of these features may be exploited to offer an extra level of control over the construction of a film scaffold by constructing a 3D matrix from highly controlled 2D film components. Such a biomaterial

matrix may find use in cornea tissue engineering in that films can be produced to guide cell and ECM production to produce individual lamellae-like tissue structures *in vitro.* These tissue structures can then be assembled at later time point *in vitro* to produce tissue construct.

3D stacked and porous silk films were successfully prepared that supported cell viability. Cells within the stacked film constructs exhibited morphologies similar to *in situ* corneal keratocytes. In addition, type I collagen was found throughout the stacked structure. This is the first successful demonstration of a multilayered film construct assembled with more than 2 layers of cultured cells. Because most tissue structures in living systems are ascribed to helicoidal organization of collagen layers, the ability to stack and control thin film features in this way, while maintaining transport in the z direction, opens up new options for complex 3D tissue formation to better mimic biological tissue structural hierarchy.

Silk fibroin offers a number of advantages to current corneal regeneration materials. First and foremost, silk films provide a mechanically robust and simplified architecture for developing corneal devices [16]. In addition, silk film formation is a relatively straightforward process [16,36]. This is not the case for other biopolymer materials such as collagen and fibrin which require more complex processing steps, and are more difficult to form into mechanically robust structures water-annealed silk films remained transparent and water stable during the study [16,20]. Surface patterning has been shown to impact corneal cell function [28,41, 54]. The results in the present work demonstrated that patterned silk films provided a suitable environment to control cell alignment and ECM synthesis, critical features in order to emulate the layered and aligned structures formed in the native cornea.

Corneal tissue engineering approaches employing acellular allograft tissue require an animal source, which establishes potential bioburden concerns [10]. Regenerated silk fibroin has been shown to have reduced bioburden content [18], while also offering the potential of acellular implantation with subsequent native tissue remodeling [18].

Silk also offers controllable biodegradation rates that can be modulated to promote extended native tissue remodeling time [18,23]. Materials such as synthetic polyglycolic acid and related polyesters, or natural collagen, degrade more rapidly or require crosslinking, and do not offer extended native tissue remodeling time when compared to silk fibroin [7]. In addition the silk films may formed with patterned, cell-guiding surfaces [20,25] and porous structures [36,52] to enhance nutrient diffusion and cell interaction amongst the layers. These added features may provide a more analogous structural environment to that found in the native cornea stroma architecture. The application of a tissue engineered corneal construct is one of many devices that could be envisioned by bringing the silk film processing methods into tissue engineering scaffold development.

5. Conclusion

Material processing techniques were established to generate silk film biomaterials for use in corneal tissue engineering. Both GFP-rCF and hCF cell lines successfully adhered, proliferated, and produced native matrix upon silk film substrates. In addition, patterned silk films were found to direct cell and actin filament alignment. Further work is needed to gain insight into how cell responses are modulated by modifying film properties. These changes will need to be correlated to understanding the mechanism of tissue development on tailored silk film substrates. Silk films that measured 2 μm in thickness and that possessed microporous structures completely through the cross-sectional area were seeded with hCF, and then stacked upon one another to form a 3D construct. Over a period of 10 days in culture hCF remained viable and appeared to have proliferated throughout the construct. In addition, initial native matrix was produced suggesting that these silk film constructs can act as scaffolding for tissue

engineering applications. Future studies to further assess matrix generation in long term culture are also needed. Such studies will provide a more complete *in vitro* characterization of these silk film biomaterial scaffolds for future application in corneal tissue engineering. The results from this study suggest that silk film substrates can be used singularly or in combination to promote corneal tissue formation depending on the desired application. Future work will aim to further elucidate how such silk film substrates may be used for regenerative medicine purposes, with a specific interest in cornea.

Acknowledgements

We are grateful to Zhiyi Cao and Noorjahan Panjwani at the Sackler Graduate School for Biomedical Sciences at Tufts University, Boston, MA for help in isolating primary rabbit corneal fibroblasts. The authors would also like to thank Laurence Daheron from the Harvard Stem Cell Institute for performing the GFP transfection of the primary rabbit corneal fibroblasts. The authors would like to extend their thanks to May Griffith at the University of Ottawa Eye Institute for contributing the human corneal fibroblasts, and to Jonathan Levitt and Catherine Chui for their technical assistance with imaging and silk materials work respectively. This work was supported by the NIH P41 Tissue Engineering Resource Center.

References

1. Eye Bank Association of America. 2005. 2005 Annual Report.
2. Georgea AJT, Larkin DFP. Corneal Transplantation: The Forgotten Graft. American Journal of Transplantation 2004;4(5):678–85. [PubMed: 15084160]
3. Nishida K, Yamato M, Hayashida Y, Watanabe K, Yamamoto K, Adachi E, et al. Corneal reconstruction with tissue-engineered cell sheets composed of autologous oral mucosal epithelium. New England Journal of Medicine 2004;351(12):1187–96. [PubMed: 15371576]
4. Ilhan-Sarac O, Akpek EK. Current concepts and techniques in keratoprosthesis. Current Opinion in Ophthalmology 2005;16(4):246–50. [PubMed: 16000898]
5. Myung D, Koh W, Bakri A, Zhang F, Marshall A, Ko J, et al. Design and fabrication of an artificial cornea based on a photolithographically patterned hydrogel construct. Biomedical Microdevices 2007;9(6):911–22. [PubMed: 17237989]
6. Griffith M, Osborne R, Hunger R, Xiong X, Doillon CJ, Laycock NLC, et al. Functional human corneal equivalents constructed from cell lines. Science 1999;286(5447):2169–72. [PubMed: 10591651]
7. Hu X, Lui W, Cui L, Wang M, Cao Y. Tissue engineering of nearly transparent corneal stroma. Tissue Engineering 2005;11(11–12):1710–7. [PubMed: 16411816]
8. Alaminos M, Sanchez-Quevedo M, Munoz-Avila JI, Serrano D, Medialdea S, Carreras I, et al. Construction of a complete rabbit cornea substitute using a fibrin-agarose scaffold. Investigative Ophthalmology & Visual Science 2006;47(8):3311–7. [PubMed: 16877396]
9. Zhang YQ, Zhang WJ, Hu XJ, Zhou GD, Cui L, Liu W, et al. Reconstruction of rabbit corneal stroma with dermal fibroblasts. MCB Molecular and Cellular Biomechanics 2006;3(4):141.
10. Liu W, Merrett K, Griffith M, Fagerholm P, Dravida S, Heyne B, et al. Recombinant human collagen for tissue engineered corneal substitutes. Biomaterials 2008;29(9):1147–58. [PubMed: 18076983]
11. Crabb RAB, Chau EP, Evans MC, Barocas VH, Hubel A. Biomechanical and microstructural characteristics of a collagen film-based corneal stroma equivalent. Tissue Engineering 2006;12(6): 1565–75. [PubMed: 16846352]
12. Torbet J, Malbouyres M, Builles N, Justin V, Roulet M, Damour O, et al. Orthogonal scaffold of magnetically aligned collagen lamellae for corneal stroma reconstruction. Biomaterials 2007;28(29): 4268–76. [PubMed: 17618680]
13. Shao Z, Vollrath F. Surprising strength of silkworm silk. Nature 2002;418(6899):741. [PubMed: 12181556]
14. Panilaitis B, Altman GH, Chen J, Jin HJ, Karageorgiou V, Kaplan DL. Macrophage responses to silk. Biomaterials 2003;24(18):3079–85. [PubMed: 12895580]
15. Arai T, Freddi G, Innocenti R, Tsukada M. Biodegradation of *Bombyx mori* silk fibroin fibers and films. Journal of Applied Polymer Science 2004;91:2383–90.

16. Jin H-J, Park J, Karageorgiou V, Kim U-J, Valluzzi R, Cebe P, et al. Water-stable silk films with reduced beta-sheet content. Advanced Functional Materials 2005;15:1241–7.
17. Meinel L, Hofmann S, Karageorgiou V, Kirker-Head C, McCool J, Gronwicz G, et al. The inflammatory responses to silk films in vitro and in vivo. Biomaterials 2005;26:147–55. [PubMed: 15207461]
18. Vepari C, Kaplan DL. Silk as a biomaterial. Progress in Polymer Science (Oxford) 2007;32(8–9): 991–1007.
19. Motta A, Fambri L, Migliaresi C. Regenerated silk fibroin films: Thermal and dynamic mechanical analysis. Macromolecular Chemistry and Physics 2002;203(10–11):1658–65.
20. Lawrence BD, Cronin-Golomb M, Georgakoudi I, Kaplan DL, Omenetto FG. Bioactive Silk Protein Biomaterial Systems for Optical Devices. Biomacromolecules 2008;9(4):1214–20. [PubMed: 18370418]
21. Zhang YQ. Natural silk fibroin as a support for enzyme immobilization. Biotechnology Advances 1998;16(5–6):961–71.
22. Wu Y, Shen Q, Hu S. Direct electrochemistry and electrocatalysis of heme-proteins in regenerated silk fibroin film. Analytica Chimica Acta 2006;558(1–2):179–86.
23. Hofmann S, Wong Po Foo CT, Rossetti F, Textor M, Vunjak-Novakovic G, Kaplan DL, et al. Silk fibroin as an organic polymer for controlled drug delivery. Journal of Controlled Release 2006;111 (1–2):219–27. [PubMed: 16458987]
24. Bettinger CJ, Cyr KM, Matsumoto A, Langer R, Borenstein JT, Kaplan DL. Silk fibroin microfluidic devices. Advanced Materials 2007;19(19):2847–50.
25. Gupta MK, Khokhar SK, Phillips DM, Sowards LA, Drummy LF, Kadakia MP, et al. Patterned silk films cast from ionic liquid solubilized fibroin as scaffolds for cell growth. Langmuir 2007;23(3): 1315–9. [PubMed: 17241052]
26. Fitton JH, Dalton BA, Beumer G, Johnson G, Griesser HJ, Steele JG. Surface topography can interfere with epithelial tissue migration. Journal of Biomedical Materials Research 1998;42(2):245–57. [PubMed: 9773820]
27. Karuri NW, Liliensiek S, Teixeira AI, Abrams G, Campbell S, Nealey PF, et al. Bilogical length scale topography enhances cell-substratum adhesion of human corneal epithelial cells. Journal of Cell Science 2004;117(15):3153–64. [PubMed: 15226393]
28. Liliensiek SJ, Campbell S, Nealey PF, Murphy CJ. The scale of substratum topographic features modulates proliferation of corneal epithelial cells and corneal fibroblasts. Journal of Biomedical Materials Research - Part A 2006;79(1):185–92. [PubMed: 16817223]
29. Loesberg WA, te Riet J, van Delft FCMJM, Scho?n P, Figdor CG, Speller S, et al. The threshold at which substrate nanogroove dimensions may influence fibroblast alignment and adhesion. Biomaterials 2007;28(27):3944–51. [PubMed: 17576010]
30. Dunn GA, Brown AF. Alignment of fibroblasts on grooved surfaces described by a simple geometric transformation. Journal of Cell Science 1986;83:313–40. [PubMed: 3805145]
31. Chen CS, Mrksich M, Huang S, Whitesides GM, Ingber DE. Geometric control of cell life and death. Science 1997;276(5317):1425–8. [PubMed: 9162012]
32. Chirila TV, Barnard Z, Zainuddin, Harkin DG, Schwab IR, Hirst LW. Bombyx mori Silk Fibroin Membranes as Potential Substrata for Epithelial Constructs Used in the Management of Ocular Surface Disorders. Tissue Engineering Part A 2008;14(7):1203–11. [PubMed: 18380593]
33. Cintron C, Covington H, Kublin CL. Morphogenesis of rabbit corneal stroma. Investigative Ophthalmology & Visual Science 1983;24:543–56. [PubMed: 6841000]
34. Ethier CR, Johnson M, Ruberti J. Ocular biomechanics and biotransport. Annul Rev Biomed Eng 2004;6:249–73. [PubMed: 15255770]
35. Doutch JJ, Quantock AJ, Smith VA, Meek KM. Light transmission in the human cornea as a function of position across the ocular surface: theoretical and experimental aspects. Biophys J. 2008 September 12;2008:biophysj.108.132316
36. Jin H-J, Park J, Valluzzi R, Cebe P, Kaplan DL. Biomaterial Films of *Bombyx Mori* Silk Fibroin with Poly(ethylene oxide). Biomacromolecules 2004;5:711–7. [PubMed: 15132651]

37. Chan KY, Patton DL, Cosgrove YT. Time-lapse videomicroscopic study of in vitro wound closure in rabbit corneal cells. Investigative Ophthalmology and Visual Science 1989;30(12):2488–98. [PubMed: 2592161]
38. Rubinson DA, Dillon CP, Kwiatkowski AV, Sievers C, Yang L, Kopinja J, et al. A lentivirus-based system to functionally silence genes in primary mammalian cells, stem cells and transgenic mice by RNA interference. Nature Genetics 2003;33(3):401–6. [PubMed: 12590264]
39. Karlon WJ, Hsu PP, Song LI, Chien S, McCulloch AD, Omens JH. Measurement of Orientation and Distribution of Cellular Alignment and Cytoskeletal Organization. Annals of Biomedical Engineering 1999;27(6):712–20. [PubMed: 10625144]
40. Bayan, C. Master of Science Thesis. Tufts University; Medford, MA, USA: 2007. Quantification of collagen fibril alignment and density in second harmonic generation images of cellular collagen matrices.
41. Xia Y, Whitesides GM. Soft lithography. Annual Review of Materials Science 1998;28(1):153–84.
42. Teixeira AI, Nealey PF, Murphy CJ. Responses of human keratocytes to micro- and nanostructured substrates. Journal of Biomedical Materials Research - Part A 2004;71(3):369–76. [PubMed: 15470741]
43. Jin H-J, Kaplan DL. Mechanism of silk processing in insects and spiders. Nature 2003;424(28):1057–61. [PubMed: 12944968]
44. Cuniberti C, Ferrando R. Electron microscope investigation of poly(ethylene oxide) supermolecular particles in solution. Polymer 1972;13(8):379–84.
45. Linsenmayer TF, Gibney E, Igoe F, Gordon MK, Fitch JM, Fessler LI, et al. Type V collagen: molecular structure and fibrillar organization of the chicken alpha 1(V) NH2-terminal domain, a putative regulator of corneal fibrillogenesis. J Cell Biol 1993 Jun;121(5):1181–9. [PubMed: 8501123]
46. Marchant JK, Hahn RA, Linsenmayer TF, Birk DE. Reduction of type V collagen using a dominant-negative strategy alters the regulation of fibrillogenesis and results in the loss of corneal-specific fibril morphology. The Journal of Cell Biology 1996;135(5):1415–26. [PubMed: 8947562]
47. Tomasek JJ, Gabbiani G, Hinz B, Chaponnier C, Brown RA. Myofibroblasts and mechano: Regulation of connective tissue remodelling. Nature Reviews Molecular Cell Biology 2002;3(5):349–63.
48. Doane KJ, Birk DE. Fibroblasts retain their tissue phenotype when grown in three-dimensional collagen gels. Experimental Cell Research 1991;195(2):432–42. [PubMed: 2070825]
49. Diehl KA, Foley JD, Nealey PF, Murphy CJ. Nanoscale topography modulates corneal epithelial cell migration. Journal of Biomedical Materials Research - Part A 2005;75(3):603–11. [PubMed: 16106433]
50. Tsukada M, Gotoh Y, Nagura M, Minoura N, Kasai N, Freddi G. Structural changes of silk fibroin membranes induced by immersion in methanol aqueous solutions. Journal of Polymer Science, Part B: Polymer Physics 1994;32(5):961–8.
51. Han B, Schwab IR, Madsen TK, Isseroff RR. A fibrin-based bioengineered ocular surface with human corneal epithelial stem cells. Cornea 2002;21(5):505–10. [PubMed: 12072727]
52. Lawrence BD, Omenetto F, Chui K, Kaplan DL. Processing Methods to Control Silk Fibroin Film Biomaterial Features. Journal of Materials Science. 2008In press

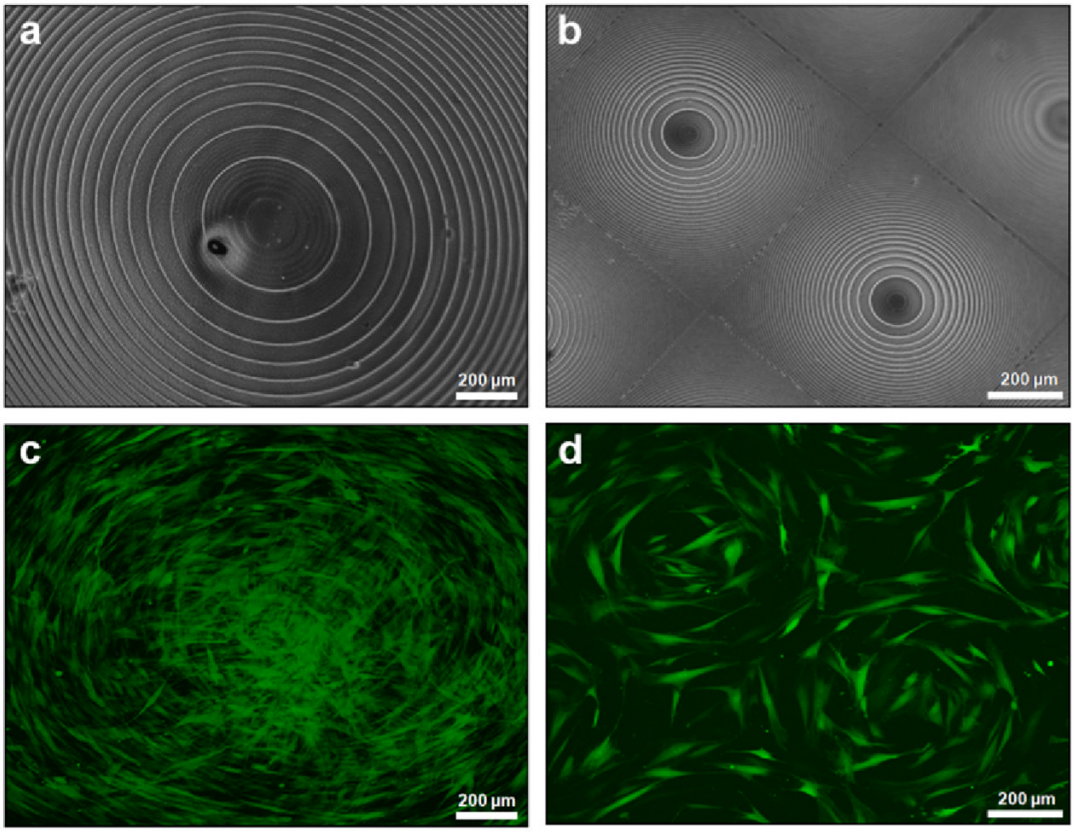

Fig. 1.
Phase contrast image of (a) 1 cm diameter and (b) multiple 700 μm diameter concentric circle silk film patterns. (c)(d) Fluorescent images of GFP-rCFs seeded on respective concentric film patterns at day 4 in culture.

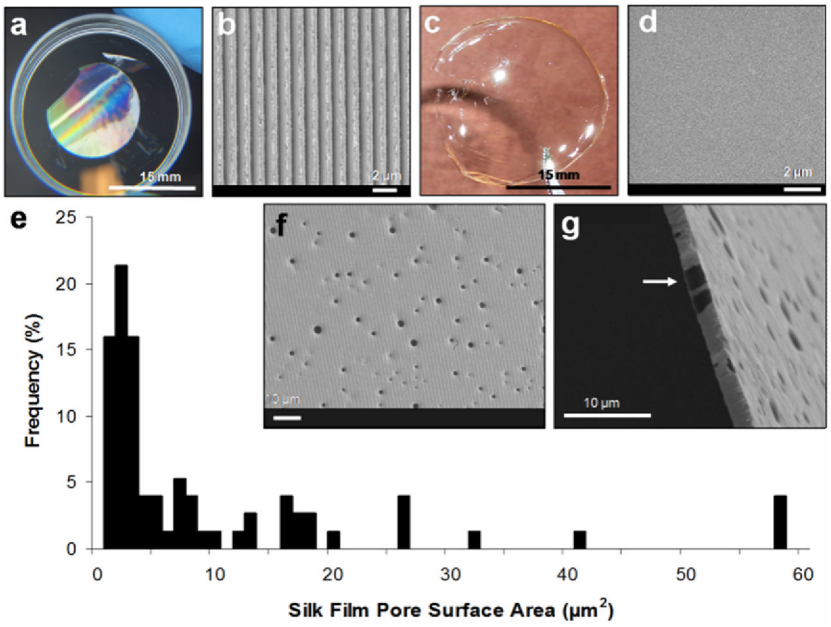

Fig. 2.

(a) Aligned grooved patterned and (c) flat silk films with respective SEM images of their surface topography (b)(d). Silk films were produced with pores measuring 500 nm to 5 μm in diameter (e) as seen from both the surface (f) and cross-sectional (g) views. Films measured 2 μm in thickness and exhibited pores throughout the entire cross-sectional area (b).

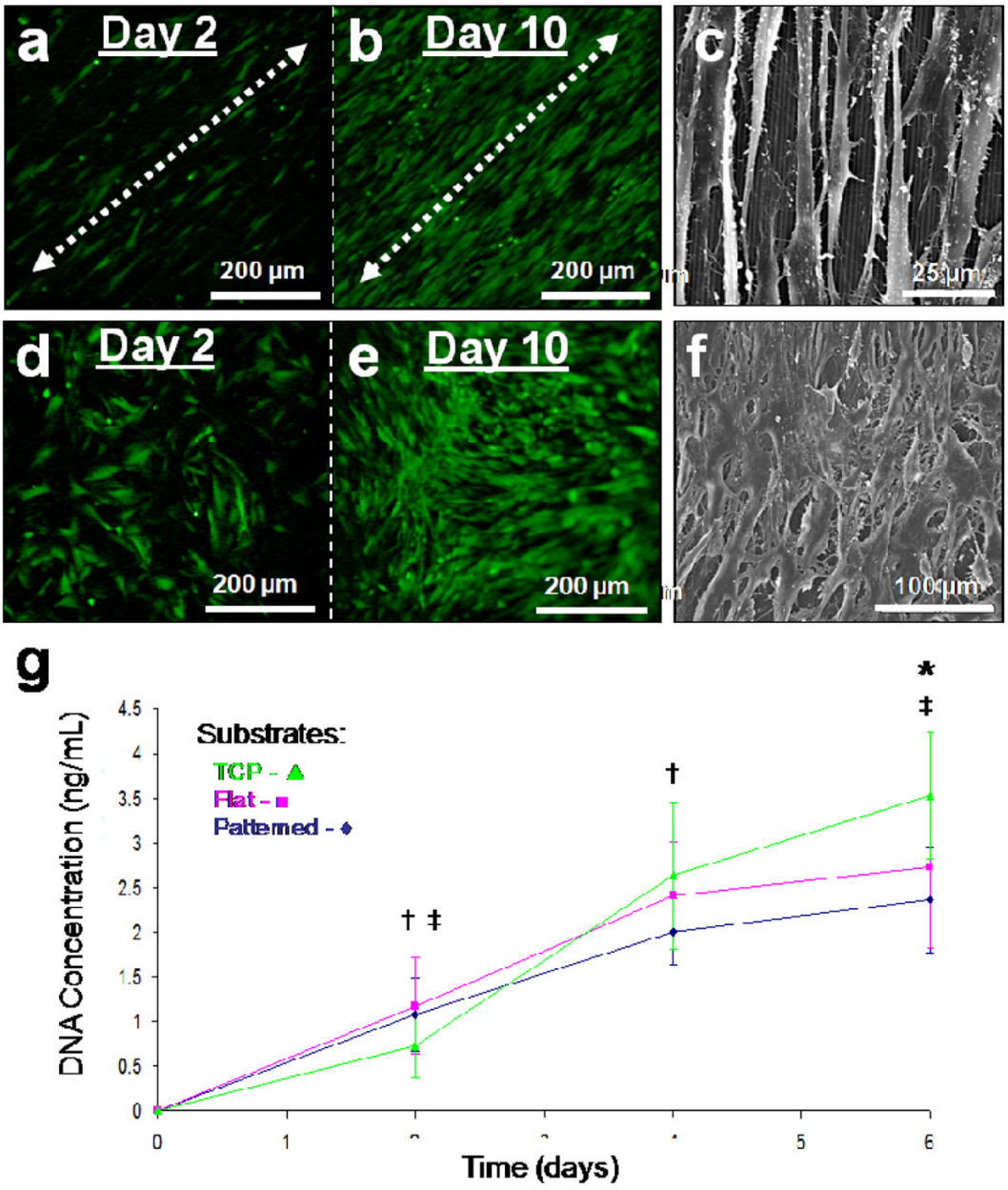

Fig. 3.

Fluorescent microscopy images of silk films seeded with GFP-rCFs at days 2 and 10 on (a,b) patterned and (d,e) flat silk film surfaces respectively. Cell alignment with the patterned groove direction (arrows) was observed upon patterned surfaces as early as day 2 in culture, while random cellular growth was found on flat surfaces. Culture confluency was reached by day 10 for both surfaces. SEM images of GFP-rCFs seeded upon (c) patterned and (f) flat silk film surfaces. SEM imaging revealed cellular alignment along the pattern axis as seen below the cell bodies (c). (g) DNA content over a 6 day culture period for GFP-rCFs was assessed for patterned silk films (◆), flat silk film (▪), and TCP (▲) substrates over a 6 day culture. † and ‡ indicate statistical significance between means of similar substrate groups at different time points ($p<0.05$, $n = 6$, and error bars = SD).

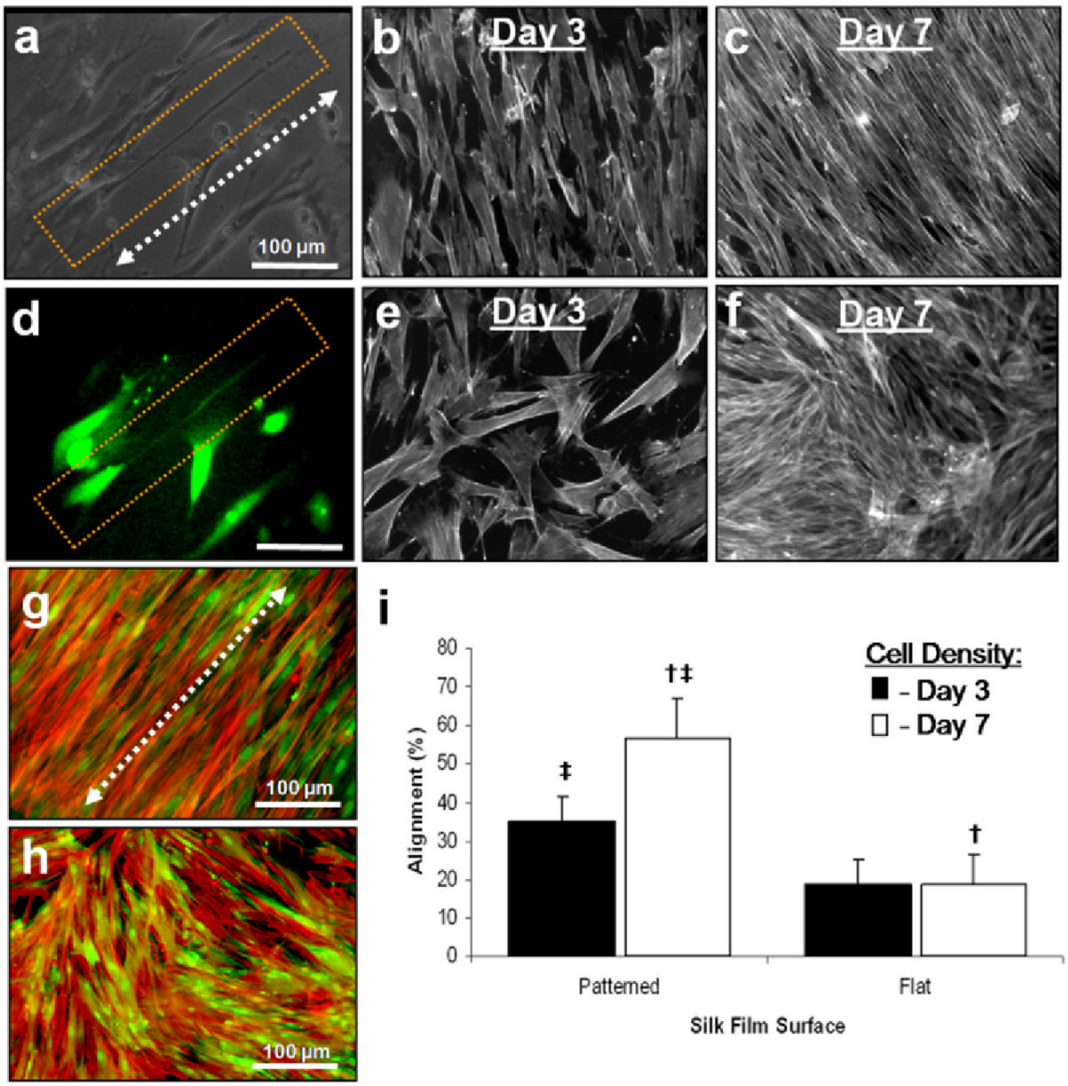

Fig. 4.

(a) Phase contrast image of a GFP-rCF cellular process highly aligned along the patterned silk film groove axis (arrow) after 4 days in culture. (b) Fluorescent image of the same cellular process indicating true cellular component. Actin staining for both (g) patterned and (h) flat silk film surfaces after 10 days in culture. Images are in false color; red indicates stained actin filaments and green represents GFP fluorescence. (i) A statistical significance between actin alignment on patterned and flat silk film surfaces was found († indicates statistical difference; $p<0.05$; error bars=SD; n=3). Fluorescent images of actin filament organization for different culture time points of GFP-rCFs seeded upon (b)(c) patterned and (e)(f) flat silk film surfaces. (b)(e) Lower cell densities exhibited greater cell spreading. At higher cell densities the cells became more compact and exhibited greater aligned organization along the silk film groove axis (c) as compared to flat silk film surfaces (f). (i) Cell density affects actin filament organization on patterned silk film surfaces. (i) A statistically significant increase in actin filament alignment is observed at increased cell densities († indicates statistical difference; $p<0.05$; error bars = SD; n=3). No affect on actin filament alignment was observed between cell density groups on flat silk film surfaces.

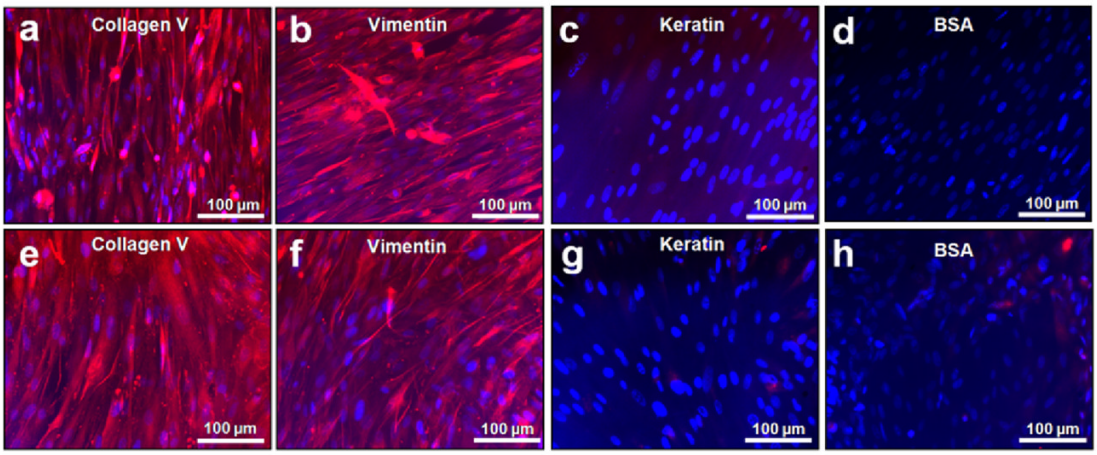

Fig. 5.

Fluorescent immunostaining of rCFs after 10 days in culture on both patterned and flat silk film surfaces. Red indicates protein of interest, while blue indicates stained nucleus using DAPI. (a)(e) Collagen V was highly expressed on both surfaces indicating the retainment fibroblast differentiation. (b)(f) Vimentin was used as positive control, (c)(g) keratin was used as a negative control for epithelium, and (d)(h) BSA was used to a control for non-specific binding to the silk film substrate.

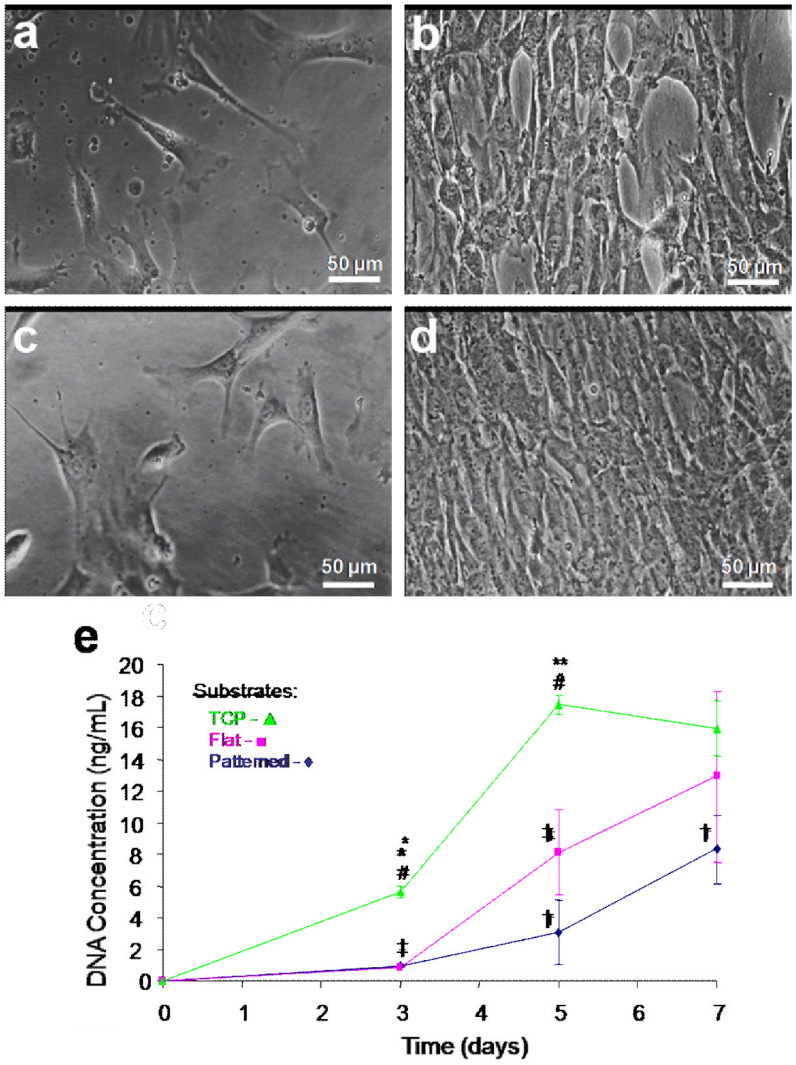

Fig. 6.

Phase contrast images of hCFs cultured upon both (a,b) patterned and (c,d) flat silk film surfaces at 3 and 7 days in culture respectively. hCF alignment upon patterned silk film surfaces was apparent at day 3 in culture, in which the cells tended to align along the patterned axis (a), as opposed to randomly spreading on flat surfaces (c). (h) DNA content was assessed for hCFs over 7 days in culture on patterned silk film (◆), flat silk film (▪), and TCP (▲) substrates over time. * and ** indicates statistical significance between means of different substrate groups at similar time points; † and ‡ indicate statistical significance between means of similar substrate groups at different time points ($p<0.05$, n = 6, and error bars = SD).

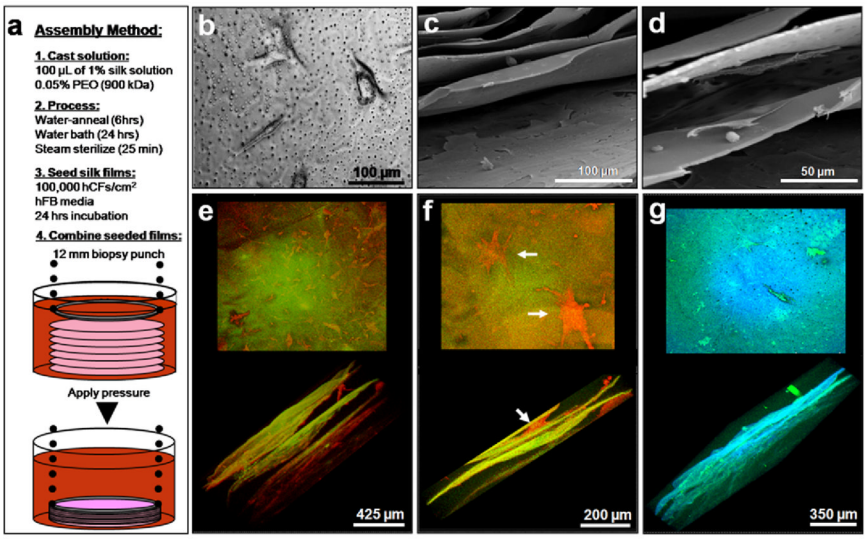

Fig. 7.

(a) Summary schematic of the assembly process for three-dimensional silk film corneal constructs on day 2 of culture. (b) hCFs seeded on porous silk film scaffolds at day 1 in culture. (c–d) SEM revealed morphological features of the stacked constructs after 7 days in culture. Cells were seen to form layers of ECM (c) and interface with various films surfaces (d). (e-g) Actin staining revealed hCF growth throughout the stacked construct at 7 days in culture (red indicates actin staining while green/orange indicates silk film substrate). (f) Higher magnification showed spread cell morphologies similar to the *in situ* corneal keratocyte phenotype (arrows). (g) Collagen type I staining of hCFs within the silk film constructs revealed tissue matrix produced throughout (green indicates collagen type I while blue indicates silk film substrate). Pore structures within the silk film structure are seen as black holes in the silk film en face view (g).